

Adaptive Sampling with the Ensemble Transform Kalman Filter. Part II: Field Program Implementation

S. J. MAJUMDAR,* C. H. BISHOP, AND B. J. ETHERTON

Department of Meteorology, The Pennsylvania State University, University Park, Pennsylvania

Z. TOTH

SAIC at Environmental Modeling Center, NCEP, NWS, NOAA, Camp Springs, Maryland

(Manuscript received 23 May 2000, in final form 24 September 2001)

ABSTRACT

The practical application of the ensemble transform Kalman filter (ET KF), used in recent Winter Storm Reconnaissance (WSR) programs by the National Centers for Environmental Prediction (NCEP), is described. The ET KF assesses the value of targeted observations taken at future times in improving forecasts for preselected critical events. It is based on a serial assimilation framework that makes it an order of magnitude faster than its predecessor, the ensemble transform technique. The speed of the ET KF enabled several different forecast scenarios to be assessed for targeting during recent WSR programs.

Each potential observational network is broken down into idealized routine and adaptive components. The adaptive component represents a predesigned flight track along which GPS dropwindsondes are released. For a large number of flight tracks, the ET KF estimates the forecast error reducing effects of these observations (via the "signal variance"). The track that maximizes the average forecast signal variance within a selected verification region is deemed optimal for targeting. Secondary flight tracks can also be chosen using serial assimilation, by calculating the signal variance for each flight track given that the primary track had already been selected.

For the second consecutive year the ET KF was able to estimate, via a statistical rescaling, the variance of NCEP signal realizations produced by the dropwindsonde data. A monotonic increasing relationship between the ET KF signal variance and the reduction in NCEP forecast error variance due to the targeted observations was then deduced for the operational 2001 WSR program.

1. Introduction

Large forecast errors over land may arise from uncertainties in the analysis within upstream regions of limited observational density. In recent winters, aircraft equipped with GPS dropwindsondes have been sent to take observations over the Atlantic and Pacific Oceans in an attempt to reduce the occurrences of such forecast failures. Typically, a 3–6-day forecast is used to identify an area (the *verification region*) where human activity is likely to be affected by significant weather such as heavy snow or rainfall at a particular time (the *verification time*). One then attempts to determine where the aircraft should take observations a day or two from now (the *targeting time*) in order to minimize the likelihood

of the significant weather event being predicted poorly by a forecast that uses the *targeted* aircraft observations in addition to the nontargeted, *routine* observations.

A variety of techniques have been employed to identify locations for deployment of targeted observations during recent field programs. These include the singular vector (SV) technique (Palmer et al. 1998; Gelaro et al. 1999; Buizza and Montani 1999; Bergot et al. 1999), the analysis sensitivity technique (Langland and Rohaly 1996; Bergot et al. 1999), the observation sensitivity technique (Baker and Daley 2000), and the quasi-linear inverse model technique (Pu and Kalnay 1999). The ensemble transform (ET) technique (Bishop and Toth 1999) was used by the Environmental Modeling Center (EMC) at the National Centers for Environmental Prediction (NCEP) during the Fronts and Atlantic Storm Track Experiment (FASTEX; Szunyogh et al. 1999a) and the North Pacific Experiment (NORPEX; Langland et al. 1999; Szunyogh et al. 1999b) investigations, and the 1999 Winter Storm Reconnaissance program (WSR99; Toth et al. 1999; Szunyogh et al. 2000). The ensemble transform Kalman filter (ETKF) was first used at NCEP during WSR99 along with the ET technique,

* Current affiliation: RSMAS/MPO, University of Miami, Miami, Florida.

Corresponding author address: Dr. S. J. Majumdar, RSMAS/MPO, University of Miami, 4600 Rickenbacker Cswy., Miami, FL 33149-1098.

E-mail: smajumdar@rsmas.miami.edu

and then exclusively during the 2000 and 2001 WSR programs. The 2001 program was the first to be fully operational at NCEP. For information on the practical implementation by the National Weather Service, and a more detailed background on previous adaptive observing programs, see Toth et al. (2001).

The ET KF is mathematically consistent with the theory of the ET technique under certain restrictive conditions. The theory of the ET KF is described in detail in Bishop et al. (2001; hereafter referred to as Part I). The two main aims of this paper are (i) to describe the operational ET KF products that are used to make flight planning decisions during WSR programs, using the theory developed in Part I, and (ii) to evaluate whether the ET KF was able to predict the reduction in NCEP forecast error variance during the 2001 WSR program.

As shown in Part I, the ET KF allows *observation sensitivity* to be specified in a theoretically more consistent way than the ET technique. It rapidly estimates the likelihood that a particular deployment of observations would significantly reduce the error of an analysis or forecast within any given geographical region. The information from all feasible deployments can then be synthesized to identify the optimal flight path. The ET KF can also use error covariance information relevant to the first chosen flight to assess the sensitivity to observations from a second flight, should one be available. It has some similarities with the observation sensitivity technique of Baker and Daley (2000) in that it explicitly accounts for the manner in which the first guess error covariances of a data assimilation scheme interpolates observational information. An advantage of Baker and Daley's technique over the ET KF is that it assumes exactly the same first guess error covariances as those assumed by the operational data assimilation scheme, whereas the ET KF assumes the error covariances of an ensemble Kalman filter (Evensen 1994; Houtekamer and Mitchell 1998, and others). Currently, there are no ensemble Kalman filters being used for operational data assimilation. On the other hand, the more rapid ET KF uses its own predictions of innovation vector covariance to translate observation sensitivity into an estimate of the reduction in forecast error variance. In contrast, Baker and Daley's technique does not yet estimate reductions in forecast error variance, although it can be made to do so by forming an outer product of the forecast aspect gradient (with respect to the innovation vector) using an innovation vector covariance matrix norm.

We call the difference between a state estimate that uses a specific set of targeted observations and one that does not a *signal realization*. At the analysis (forecast) time, this signal corresponds to the difference between analyses (forecasts) that use and do not use the targeted observations. The signal can be viewed as a stochastic process whose variations are described by a *signal covariance matrix*. Its diagonal terms give the variance of stochastic signal realizations that would be obtained by

assimilating a specific set of targeted observations with the ET KF. If background and observational error covariances are accurately specified and errors evolve linearly, the signal variance is equal to the reduction in error variance due to the targeted observations. The latter quantity is a key product that the ET KF attempts to predict. In the current formulation of the ET KF used at NCEP, estimates of error variance reduction are less than ideal for several reasons. These include the size and age of the ensembles used to estimate background error covariances, the exclusion of intervening observational networks up to and including the targeting time, the differences between covariances assumed by the ET KF and NCEP's operational three-dimensional variational data assimilation scheme (3DVAR) (Parrish and Derber 1992), and the assumption that the ET KF uses linear combinations of nonlinear forecasts. Despite these caveats, the ET KF has proved capable of directing dropwindsonde-equipped aircraft to locations that improve forecasts within the downstream verification region (Szunyogh et al. 2000). Additionally, tests have shown that data taken outside the target region selected by ensemble transform methods produced a weaker NCEP forecast signal within the verification region at the verification time than signals produced by data collected within the target region (e.g., see Toth et al. 2000). Further quantitative "data denial" tests of the optimality of target regions selected by the ET KF are still required.

A linear, increasing relationship between the ET KF predicted signal variance and the variance of NCEP signals¹ produced during the 2000 WSR program has been found statistically at both the targeting and verification times (Majumdar et al. 2001). Via a rescaling factor, a monotonically increasing relationship between the ET KF signal variance and the reduction in NCEP forecast error variance was then deduced. While Majumdar et al. (2001) used horizontal wind components in their calculations (since only these variables were used up to and including the 2000 WSR program), in this paper we present the formulation of ET KF products that include the effects of observing wind and temperature, and a total energy signal variance that was used operationally during the 2001 WSR program.

In section 2, the adjustments to the theory presented in Part I that were required to implement the ET KF within an operational framework are described. The synthesis of ET KF signal variance estimates for all possible deployments of targeted observations to identify the best deployment is described in section 3. The use of serial assimilation in deploying multiple aircraft is also illustrated in this section. In section 4, the ability of the ET

¹ An NCEP signal is defined here by the difference between two parallel medium-range forecast model (MRF) analysis-forecast cycles. One cycle assimilated the routine and targeted observations at each analysis time, whereas the other cycle assimilated only the routine observations at each analysis time. For more details, see Szunyogh et al. (1999a, 2000).

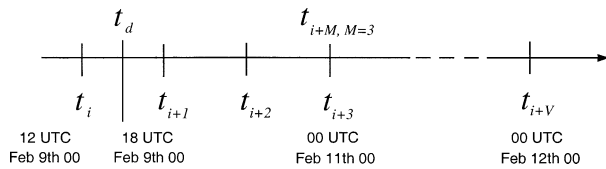


FIG. 1. Times involved in the decision-making process. The objective is to improve a forecast initialized at t_{i+M} within a selected verification region at time t_{i+V} . The decision to deploy adaptive observations at time t_d must be made at least 1 day before time t_{i+M} , based on an ensemble initialized at time t_i . Ideal times are given for targeting on 11 Feb 2000 to improve a 24-h forecast; however, various constraints prevent the possibility of using a 36-h-old ECMWF ensemble during WSR programs. A 48–60-h-old ensemble is often employed in practice. Time steps are of 12 h, corresponding to analysis times of the MRF model.

KF to predict NCEP signal variance and reduction in NCEP forecast error variance is assessed for the 2001 WSR program. Concluding remarks are given in section 5.

2. The ET KF formulation for adaptive sampling

During adaptive observing programs, a potentially important weather event is identified between 3 and 6 days in advance of its likely occurrence over land at verification time t_{i+V} (Fig. 1). Using the most recently available ensemble, initialized at time t_i , the aim is to identify optimal deployments of supplementary observations at least a day in advance of the deployments. In Part I, the theory was developed for all available sets of adaptive observations over M intervening times t_{i+1} , t_{i+2} , \dots , t_{i+M} . In current targeting programs, only one such targeting time t_{i+M} is used in the ET KF calculations (where $M < V$). Typically t_{i+M} is 36–60 h after t_i . The targeted data collected by the GPS sondes are assimilated into the operational models at time t_{i+M} , together with routine observations from around the globe. The routine observational network comprises all regular observations (e.g., from rawinsondes, satellites, etc.), which are assimilated into the global models on a 6-hourly basis. This means that there are 6–10 routine observational networks deployed between t_i and t_{i+M} , which are not accounted for in the present operational formulation.

Each observational network is divided into two components in our formulation. The first is a simplified routine component (denoted by superscript r) with $p^r = O(10^5)$ “observations” taken at the targeting time t_{i+M} , and the second is an adaptive component that contains $p^a = O(10^3)$ targeted observations taken at t_{i+M} .² We first estimate a new *routine analysis error covariance matrix* valid for the routine observations. The analysis and forecast error covariance reducing effect of all Q

sets of targeted observations, entitled the signal covariance matrix, is then rapidly estimated, using serial assimilation to take advantage of the fact that $p^a \ll p^r$. In serial assimilation (described in detail in Part I), observations are assimilated in groups, with the background error covariance matrix being updated after each group is assimilated. The diagonal terms of the signal covariance matrix are the main products used to identify optimal locations for targeted observations.

a. Error covariances for the routine observational network

In ensemble Kalman filters (Evensen 1994; Houtekamer and Mitchell 1998), forecast (background) error covariance matrices are approximated by the outer product of ensemble perturbations that are valid 6–12 h after the ensemble generation time. Due to the logistics of flight planning and availability of ensembles, the operational ET KF can only use ensemble forecasts that are valid at least 36 h after the initialization time t_i . In Part I, we showed how the ET KF could be used to simulate the effect on forecast error variance of intervening observational networks between times t_i and t_{i+M} . However, certain aspects of these routine observational networks such as the location and quality of cloud track wind vectors and Television and Infrared Observation Satellite (TIROS) Operational Vertical Sounder (TOVS) radiances cannot be known ahead of time, and the true NCEP observation operator has not yet been imported into the targeting code. To make the scheme practicable in the face of these difficulties, the analysis error covariance matrix at time t_{i+M} is crudely estimated as an outer product of the matrix containing transformed ensemble perturbations, ignoring the intervening observational networks. The K columns of the $N \times K$ matrix $\mathbf{X}(t_{i+M} | H_i^r)$ contain K perturbations of length N , valid at time t_{i+M} . The notation $\mathbf{X}(t_{i+M} | H_i^r)$ is motivated by the fact that the state of the ensemble perturbations is conditional upon the routine observations associated with the nonlinear observation operator H_i^r that were assimilated at the initialization time t_i . The ensemble perturbations are transformed via the $K \times K$ matrix \mathbf{T}^r to give a new set of perturbations that are orthonormal with respect to an inverse analysis error variance norm, and consistent with current analysis error variance estimates. This is achieved by requiring that

$$\mathbf{T}^{rT} \mathbf{X}^T(t_{i+M} | H_i^r) \mathbf{D}_A^{-1}(\hat{\mathbf{H}}^r) \mathbf{X}(t_{i+M} | H_i^r) \mathbf{T}^r = \mathbf{I}, \quad (1)$$

where the $N \times N$ diagonal matrix $\mathbf{D}_A^{-1}(\hat{\mathbf{H}}^r)$ lists the inverse of the best available estimates of analysis error variance at time t_{i+M} , multiplied by the constant K/N . Here, $\hat{\mathbf{H}}^r$ is the linearized observation operator associated with the routine observations. To satisfy (1), the k th column of \mathbf{T}^r is set equal to the k th eigenvector of the $K \times K$ symmetric matrix $\mathbf{X}^T(t_{i+M} | H_i^r) \mathbf{D}_A^{-1}(\hat{\mathbf{H}}^r) \mathbf{X}(t_{i+M} | H_i^r)$, scaled by $\sqrt{1/\lambda_k}$, where λ_k is the corresponding eigenvalue. The routine

² In the ET KF targeting strategy, actual observations are not used since they are not known in the future. Error covariances from simplified routine and targeted observations are used in the ET KF.

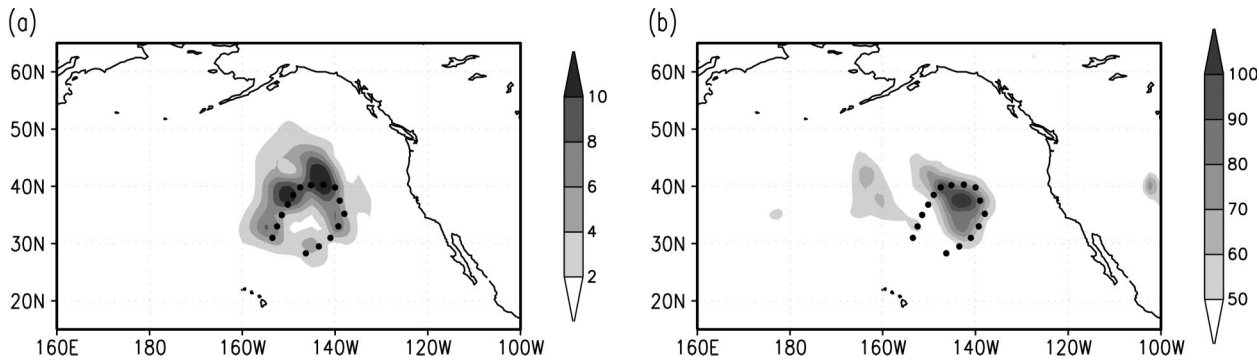


FIG. 2. (a) Squared NCEP signal in J kg^{-1} at targeting time 0000 UTC 11 Feb 2000, averaged over the 850-, 500-, and 200-hPa pressure levels. It is calculated as $(1/2)[(u^q - u^r)^2 + (v^q - v^r)^2] + 3.346 (T^q - T^r)^2$, where (u^q, v^q, T^q) and (u^r, v^r, T^r) represent NCEP analyses of horizontal wind components and temperature with and without the targeted observations, respectively. Dots represent locations at which GPS sondes were released. (b) ET KF signal variance at 0000 UTC 11 Feb 2000. Units are J kg^{-1} for all signal variance plots. A combined ensemble of 25 ECMWF members (generated +36 h prior to the targeting time) and 7 NCEP members (+24 h, +36 h) is used in this calculation.

analysis error covariance matrix $\mathbf{P}(t_{i+M} | \hat{\mathbf{H}}^r)$, conditional on $\hat{\mathbf{H}}^r$, is then given as the outer product of transformed ensemble perturbations,

$$\mathbf{P}(t_{i+M} | \hat{\mathbf{H}}^r) = \mathbf{X}(t_{i+M} | H_i^r) \mathbf{T}^r \mathbf{T}^{rT} \mathbf{X}^T(t_{i+M} | H_i^r). \quad (2)$$

During the 2001 WSR program, the variables used in $\mathbf{X}(t_{i+M} | H_i^r)$ consisted of temperature and horizontal wind components at 2.5° resolution, at the 850-, 500-, and 200-hPa pressure levels. More variables and pressure levels may be included in future programs. The diagonal values of $\mathbf{D}_A^{-1}(\hat{\mathbf{H}}^r)$ (given as the inverse square of the terms in Table 1) are taken from NCEP's fit to the analysis to observed data averaged in the Northern Hemisphere over February 2000 (S. Saha 1999, personal communication). While we emphasize that this quantity does not represent analysis error variance, it was all that was available at NCEP and was assumed to give a reasonable estimate. Furthermore, the values in Table 1 are consistent with the Naval Research Laboratory's estimates of globally and temporally averaged analysis error variance (R. Gelaro 2000, personal communication). The sensitivity of ET KF targeting results to moderate changes in these estimates is negligibly low.

During the 2001 WSR program, a combined ensemble of 25 European Centre for Medium-Range Weather Forecasts (ECMWF) members (Molteni et al. 1996; Buizza et al. 1998) and 10 NCEP Medium Range Fore-

cast (MRF) members (Toth and Kalnay 1997) was used. The number of ensemble members K (35) is much smaller than the length of the state vector N (94608). Hence, since we are restricted to working within the subspace of ensemble perturbations, the error covariance matrix estimates are rank deficient. However, the ensembles are generated with the intention that perturbations project significantly onto leading structures of error in the atmosphere in the medium range. We therefore expect that the suboptimal ET KF is still capable of identifying the regions from which dominant error structures propagate toward the verification region.

b. Error covariances for the adaptive observational network

The ET KF attempts to predict the covariance of *signal realizations* produced by Q possible deployments of supplementary observations. A signal realization is defined by the difference between analyses (or forecasts) initialized with and without the targeted observations. An example of the square of an NCEP signal realization at time t_{i+M} is shown in Fig. 2a for a flight at 0000 UTC 11 February 2000. It represents the square of the difference between two NCEP 3DVAR analyses (Parrish and Derber 1992): one using the fully supplemented observational network, and the other using data only from the routine network. The NCEP signal attains its highest magnitudes in regions close to the observation sites. As discussed in Szunyogh et al. (1999a,b, 2000) and Toth et al. (2000, 2001), the time evolution of operational forecast signals is an important test of the success of a deployment of targeted observations.

The signal covariance matrix $\mathbf{S}(t_{i+M} | \mathbf{H}^q)$ is defined by the expected outer product of signal realizations that would be produced by the q th deployment of supplementary observations if they were assimilated using error covariances of an ET KF. As introduced in appendix B of Part I, the term \mathbf{H}^q is used to denote the observation

TABLE 1. Observation errors and analyses fit to observations assumed by the ETKF during the 2001 WSR program. Analyses fit to observations are averaged in the Northern Hemisphere over Feb 2000 (S. Saha 1999, personal communication).

Height (hPa)	Obs error		Analysis fit to obs	
	Rms wind (m s ⁻¹)	Temperature (K)	Rms wind (m s ⁻¹)	Temperature (K)
850	2.40	0.8	2.72	1.22
500	2.80	0.8	3.16	0.92
200	2.95	1.2	4.66	1.82

operator associated with the combined observational network of the routine component (p^r observations, denoted by the operator $\hat{\mathbf{H}}^r$) plus the q th feasible adaptive component (p^q observations, denoted by the operator $\hat{\mathbf{H}}^q$). These observation operators use a linear interpolation scheme to transform grid points onto observation locations. Using the serial assimilation theory of Part I, the analysis error covariance matrix $\mathbf{P}(t_{i+M} | \mathbf{H}^q)$ for the q th combined observational network is then expressed as

$$\begin{aligned} \mathbf{P}(t_{i+M} | \mathbf{H}^q) &= \mathbf{P}(t_{i+M} | \hat{\mathbf{H}}^r) \\ &\quad - \mathbf{P}(t_{i+M} | \hat{\mathbf{H}}^r) \hat{\mathbf{H}}^{qT} [\hat{\mathbf{H}}^q \mathbf{P}(t_{i+M} | \hat{\mathbf{H}}^r) \hat{\mathbf{H}}^{qT} + \hat{\mathbf{R}}^q]^{-1} \\ &\quad \times \hat{\mathbf{H}}^q \mathbf{P}(t_{i+M} | \hat{\mathbf{H}}^r) \\ &= \mathbf{P}(t_{i+M} | \hat{\mathbf{H}}^r) - \mathbf{S}(t_{i+M} | \mathbf{H}^q), \end{aligned} \quad (3)$$

where $\hat{\mathbf{R}}^q$ is the diagonal observational error covariance matrix, whose values are displayed in Table 1. These values are the same as those assumed by NCEP's data assimilation scheme (Wu and Joo 1996). Assuming that the targeted observation and routine analysis error covariances are both specified accurately and uncorrelated with each other, (3) indicates that the signal covariance is equal to the reduction in analysis error covariance due to the q th deployment of supplementary observations. The signal covariance can be reexpressed in a computationally simple form for use in operational targeting:

$$\mathbf{S}(t_{i+M} | \mathbf{H}^q) = \mathbf{X}(t_{i+M} | H_i^r) \mathbf{V}^q \mathbf{V}^{qT} \mathbf{X}^T(t_{i+M} | H_i^r), \quad (4)$$

where the matrix $\mathbf{V}^q = \mathbf{T}^r \mathbf{C}^q [\mathbf{\Gamma}^q (\mathbf{\Gamma}^q + \mathbf{I})^{-1}]^{1/2}$, and \mathbf{C}^q and $\mathbf{\Gamma}^q$ are $K \times K$ matrices containing eigenvectors and eigenvalues of the matrix product $\mathbf{T}^{rT} \mathbf{X}^T(t_{i+M} | H_i^r) \mathbf{H}^{qT} \hat{\mathbf{R}}^{q-1} \hat{\mathbf{H}}^q \mathbf{X}(t_{i+M} | H_i^r) \mathbf{T}^r$. Using (3), (4), and the linearized dynamics operator $\mathbf{M} \equiv \mathbf{M}(t; t_{i+M})$ with a twist, the analysis error covariance matrix for the combined (routine plus targeted) observational network $\mathbf{P}(t_{i+M} | \mathbf{H}^q)$ is propagated from time t_{i+M} to time t (where $t \geq t_{i+M}$) to give

$$\mathbf{P}(t | \mathbf{H}^q) = \mathbf{M} \mathbf{P}(t_{i+M} | \mathbf{H}^q) \mathbf{M}^T + \mathbf{Q} \quad (5a)$$

$$\begin{aligned} &= \mathbf{M} \mathbf{P}(t_{i+M} | \hat{\mathbf{H}}^r) \mathbf{M}^T + \mathbf{Q} \\ &\quad - \mathbf{M} \mathbf{S}(t_{i+M} | \mathbf{H}^q) \mathbf{M}^T \end{aligned} \quad (5b)$$

$$\begin{aligned} &= \mathbf{P}(t | \hat{\mathbf{H}}^r) \\ &\quad - \mathbf{M} \mathbf{X}(t_{i+M} | H_i^r) \mathbf{V}^q \mathbf{V}^{qT} \mathbf{X}^T(t_{i+M} | H_i^r) \mathbf{M}^T \end{aligned} \quad (5c)$$

$$= \mathbf{P}(t | \hat{\mathbf{H}}^r) - \mathbf{X}(t | H_i^r) \mathbf{V}^q \mathbf{V}^{qT} \mathbf{X}^T(t | H_i^r) \quad (5d)$$

$$= \mathbf{P}(t | \hat{\mathbf{H}}^r) - \mathbf{S}(t | \mathbf{H}^q), \quad (5e)$$

where $\mathbf{Q} \equiv \mathbf{Q}(t; t_{i+M})$ is the covariance matrix of model errors accrued between times t_{i+M} and t . The twist appears in Eqs. (5c) and (5d) where the linear forward propagation of ensemble perturbations, given by $\mathbf{M} \mathbf{X}(t_{i+M} | H_i^r)$ in (5c), has been replaced by the pertur-

bations $\mathbf{X}(t | H_i^r)$ of *nonlinear* forecasts valid at time t . This saves a huge amount of computational expense because the ensemble perturbations are available for free after the ensemble has been generated, while no tangent linear propagator needs to be used in the ET KF calculations. Note that the expression for $\mathbf{S}(t | \mathbf{H}^q)$ is independent of model error and hence, in principle, it is easier for the ET KF to predict signal covariance than forecast error covariance.

The diagonal terms of $\mathbf{S}(t | \mathbf{H}^q)$ give the *signal variance* at each grid point for the q th deployment of targeted observations. To obtain an overview of the information associated with all eigenvectors of $\mathbf{S}(t | \mathbf{H}^q)$, we plot the geographical distribution of vertically averaged signal variance at the targeting time t_{i+M} . The signal variance at each point is expressed in terms of the total perturbation energy $(1/2)(u'^2 + v'^2) + 3.346 T'^2$, averaged over the 850-, 500-, and 200-hPa levels. The variables (u' , v' , T') represent transformed horizontal wind component and temperature perturbations given in the $\mathbf{X}(t | H_i^r) \mathbf{V}^q$ matrix.³ This total energy norm is consistent with that used at ECMWF in their singular vector calculations (R. Buizza 1999, personal communication). The ET KF signal variance for the flight track of Fig. 2a is shown in Fig. 2b. The maximum of signal variance lies within the horseshoe of observation locations in this case, indicating that the signal that would be obtained from an ET KF data assimilation scheme is most likely to be highest at this location if such a flight were to take place. In fact, the NCEP signal was maximized very close to the observation locations (Fig. 2a). This collocation of signal maxima with observation locations is commonly produced by NCEP's 3DVAR scheme (Parrish and Derber 1992), which assumes quasi-isotropic background error covariances.

The magnitude of the estimated ET KF signal variance in Fig. 2b and the square of the operational signal in Fig. 2a differ considerably. One should recall that while Fig. 2a depicts a signal realization, Fig. 2b depicts a signal variance. Since (if one assumes normal error statistics) the most probable signal realization amplitude is zero, the fact that the ET KF variance magnitude is much greater than the squared NCEP signal does not necessarily mean that the ET KF has overestimated the signal variance. To determine whether the ET KF signal variance estimates are too large or too small, one must examine a large number of cases. In Majumdar et al. (2001), it was found (and confirmed in section 4 of this paper) that the ET KF overestimated the variance of NCEP signal realizations by an order of magnitude during the 2000 WSR program, and they discuss several possible reasons for this overestimation. Among these

³ The upper-tropospheric variables are important in a verification norm since the targeted data often produce a significant impact on forecasts at these levels. These variables are also often closely linked, with a time delay, to weather activity at the surface. Surface variables will be added in future WSR programs.

reasons is inherent inaccuracies in estimating the routine error covariance magnitudes discussed in the previous subsection.

Note also that the maxima in Figs. 2a and 2b are not quite at the same location. This is primarily because error correlations assumed by the ET KF are different from those assumed by the quasi-isotropic 3DVAR data assimilation scheme. If the ET KF targeting technique were to be used in tandem with an operational flow-dependent data assimilation scheme such as 4DVAR (e.g., Rabier et al. 2000) or a hybrid Kalman filter (Hammill and Snyder 2000), the ET KF would likely better estimate operational error covariance matrices than it does with NCEP's current operational 3DVAR data assimilation scheme.

Various investigations (Houtekamer and Derome 1994; Buizza 1995; Gilmour et al. 2001, and others) have suggested that the linear regime may only be valid for forecasts of synoptic-scale disturbances lasting between 12 h and 3 days. Adjoint-based adaptive observing techniques [such as targeted singular vectors; Palmer et al. (1998)] assume that perturbations evolve linearly, but nevertheless they have proven to be successful in targeting on synoptic scales (Bergot 1999; Gelaro et al. 1999, 2000; Langland et al. 1999; Buizza and Montani 1999). The ET KF differs from adjoint-based techniques in that it assumes that nonlinear perturbations can be combined linearly. Tests are still required on the flow regimes and timescales under which this assumption is valid. Notwithstanding the lack of such tests, the ET KF has demonstrated skill in predicting signal variance during the 2000 and 2001 WSR programs (Majumdar et al. 2001, and section 4 of this paper). The question of how the ET KF can continue to make quantitatively reliable predictions within a nonlinear regime is beyond the scope of this paper.

c. Speeds of ET KF and ET techniques contrasted

The ET KF is only required to transform the ensemble perturbations once for a large observational network (the routine network). It then rapidly calculates the signal variance for the Q hypothetical sets of adaptive observations using $K \times K$ matrix transformations and eigenvalue calculations. In contrast, the ET technique of Bishop and Toth (1999) solves a similar relation to (1) for each of the Q observational networks, changing the equivalent of the $N \times N$ matrix $\mathbf{D}_A^{-1}(\hat{\mathbf{H}}^q)$ for each set of targeted observations. For the calculations described in this paper, $K = O(10^1)$ and $N = O(10^5)$. Hence, the ET KF is more efficient in both computational time and memory than the ET technique. The two techniques are mathematically equivalent under restrictive conditions; a proof is given in the appendix. The speed of the ET KF enables targeting calculations to be performed for several different targeting times, verification regions, and verification times during the WSR programs. It is necessary to do this to choose the best day to deploy

the aircraft, depending on the availability of resources and importance of the forecast (Toth et al. 2001). To choose the optimal deployment, signal variance calculations for each of $Q = 231$ hypothetical adaptive deployments are produced for each forecast scenario. In total, these 231 calculations take less than a minute of CPU time on the IBM SP supercomputer at NCEP, roughly 15 times faster than the ET technique. The ET KF uses an operational ensemble of forecasts initialized between 36 and 60 h before the targeting time; no extra model runs are required.

3. Summary maps and bar charts of signal variance

Although the faster speed of the ET KF relative to the ET and other targeting techniques is useful, the major practical advantage of the ET KF is that it explicitly estimates the effect of observations on forecast error variance. This enables a suite of targeting products that are the subject of this section.

a. Summary maps

Summary maps synthesize signal variance calculations for a large number of different hypothetical adaptive observational networks, using the appropriate matrix $\hat{\mathbf{H}}^q$ to map grid points onto targeted observation locations for each deployment. Here we describe the construction of such maps, using a retrospective example from the NORPEX experiment, to design the optimal flight track.

At $t_{i+M} = 0000$ UTC 5 February 1998, aircraft-borne sondes were available for deployment to improve the 24-h forecast of a storm threatening the Californian coast at $t_{i+V} = 0000$ UTC 6 February 1998. We use a 25-member ECMWF ensemble generated at $t_i = 1200$ UTC 3 February 1998 in this example. Suppose, for the moment, that our adaptive observing component consisted of nine adjacent "pseudosondes" that only measured temperature and horizontal wind components at 850, 500, and 200 hPa. Using (4), we plot the ET KF estimated total energy signal variance at the targeting time for one such "test probe" centered at 47.5°N, 172.5°E (Fig. 3a). The highest signal variance is located near the observation sites. We then use the evolved ensemble perturbations in (5d) to evaluate the signal variance at time t_{i+V} (Fig. 3b). There is little amplitude within the verification region, which suggests that this deployment of nine observations would be unlikely to improve a 24-h forecast significantly within the intended region.

Suppose now that we moved our test probe to a location centered at 35°N, 130°W (Fig. 3c). The corresponding signal variance at the targeting time is relatively large near the targeting location compared with Fig. 3a, and its maximum lies in the vicinity of a frontal zone at the targeting time (Fig. 4c). At the verification

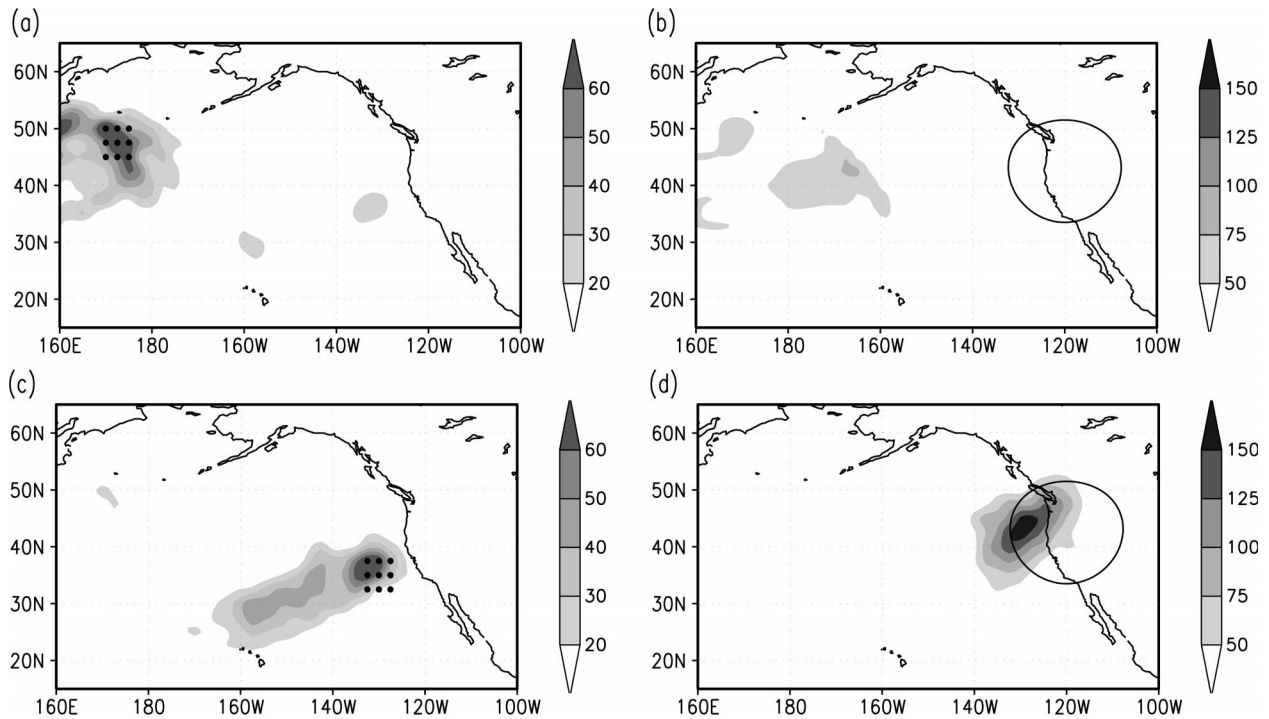


FIG. 3. (a) Signal variance for nine observations centered at 47.5°N , 172.5°E , at the targeting time 0000 UTC 5 Feb 1998. (b) As for (a) but at the verification time 0000 UTC 6 Feb 1998. The circular verification region over the western United States is shown. (c) Signal variance for nine observations centered at 35°N , 130°W , at the targeting time 0000 UTC 5 Feb 1998. (d) As for (c) but at the verification time.

time t_{i+v} , a focused maximum of signal variance lies within the verification region (Fig. 3d), and is of much higher magnitude than the signal variance of Fig. 3b. The ET KF therefore suggests that second test probe is therefore more likely to benefit a 1-day forecast within the verification region than the first probe.

A good ET KF data assimilation scheme would produce an analysis increment (or signal) in regions where errors covary significantly with errors at observation locations. In this situation, information from the innovation vector would then most likely be interpolated along the frontal zone. However, we also note that the rank deficiency of the routine analysis error covariance estimate in our suboptimal ET KF might lead to spurious correlations between the signal variance at the observation locations in Fig. 3c and that in the frontal region upstream. Regardless of whether the elongated ET KF signal variance structure is due to actual or spurious correlations, the structure is likely to be very different from a signal structure that would be produced by the operational 3DVAR scheme at NCEP (Parrish and Derber 1992). A 3DVAR signal would generally be localized in the vicinity of the observation sites due to the quasi-isotropic nature of the error covariances assumed by the data assimilation scheme. The differences between signal structures produced by an ET KF and 3DVAR may compromise the ability of an ET KF to predict the variance of NCEP signals.

For any deployment of supplementary observations denoted by q , we average the signal variance within the verification region at time t_{i+v} to focus on the likelihood of these observations to reduce forecast error in the area where the forecast is of most concern. Mathematically, this average σ^q is the trace of the signal covariance matrix localized within the verification region:

$$\sigma^q = \text{Tr}[L_V \mathbf{S}(t_{i+v} | \mathbf{H}^q)], \quad (6)$$

where L_V is the operator that localizes and vertically averages covariances within the verification region. We move the test probe to adjacent locations 5° apart (in both latitude and longitude) over the northern Pacific, and rapidly calculate σ^q for each of the $Q = 231$ possible probes [similar to the techniques of Bishop and Toth (1999), and Part I]. In Fig. 4a, σ^q is plotted as a function of the centroid location of each probe in a *summary map*. By traversing the region of maximum σ^q on the summary map (darkest shading in Fig. 4a), a suitable flight path can be designed to maximize the likelihood of reducing forecast error (assuming that error covariances are accurately specified). To illustrate how the summary map is related to the signal variance plots of Figs. 3a–d, note that the test probe shown in Fig. 3c lies within an area where a high value of σ^q is expected within the verification region. Accordingly, Fig. 3d exhibits high values of signal variance within the verification region and it is precisely these values that are

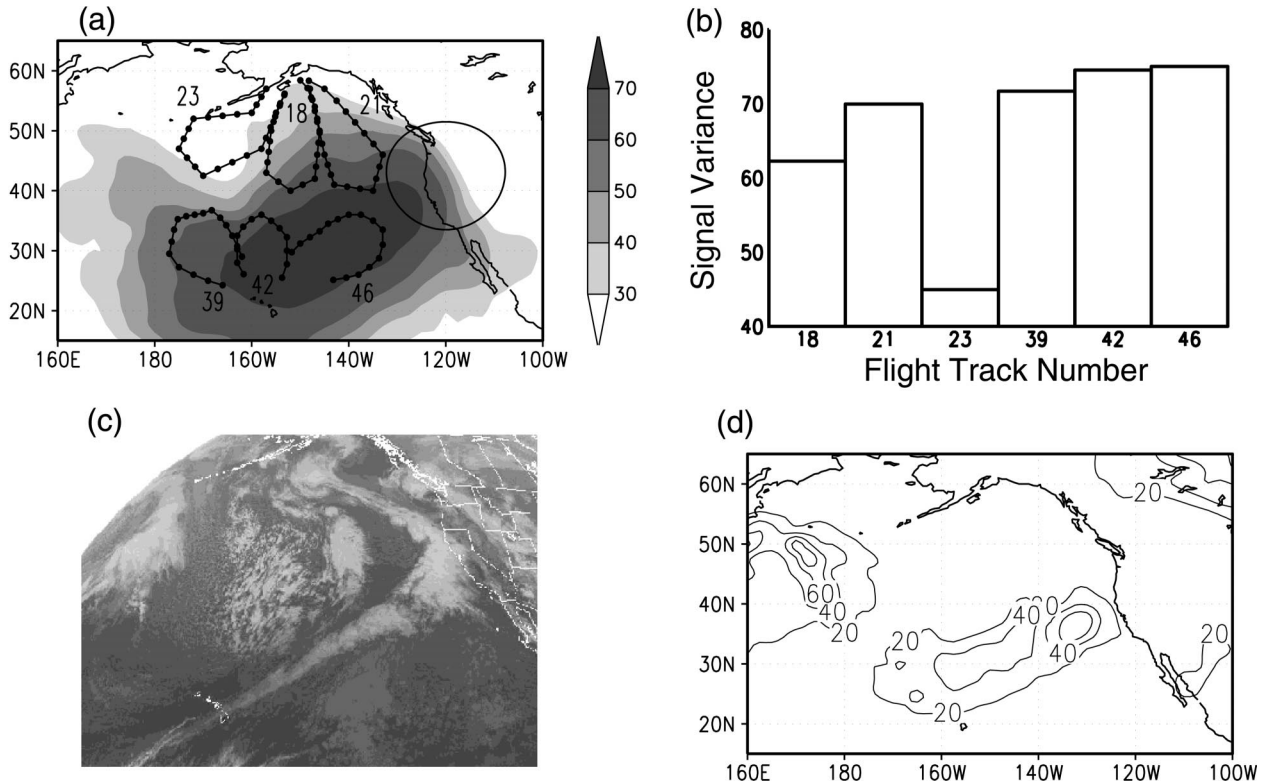


FIG. 4. (a) Summary map of average signal variance σ^q for targeting time 0000 UTC 5 Feb 1998, and verification time 0000 UTC 6 Feb 1998. (b) Bar chart of σ^q for six flight tracks displayed in (a). (c) GOES-9 infrared satellite image of northern Pacific Ocean at 0000 UTC 5 Feb 1998. (Image obtained from the NCDC Historical GOES Browse Server.) (d) Routine analysis error variance calculated from transformed 36-h-old ECMWF ensemble perturbations $\mathbf{X}(t_{i+M} | H_i)\mathbf{T}$, valid at 0000 UTC 5 Feb 1998.

averaged to give σ^q . On the other hand, the deployment shown in Fig. 3a is expected to be poor compared with the majority of other available probes of nine observations over the northern Pacific. This can also be deduced by comparing Fig. 3b with similar signal variance maps at time t_{i+V} for differently located probes.

In a similar manner, the ET KF can be used to calculate σ^q rapidly for any given flight track, and the track that maximizes this quantity is deemed optimal for targeting. As discussed in Toth et al. (1999), the quick evaluation of σ^q expedites the flight planning process. Overlaying the summary map (Fig. 4a) are six tracks, which were among the prespecified tracks used during the WSR00 program (Fig. 6a). We deduce from Fig. 4b that tracks 42 and 46 out of Honolulu are the best of these six deployments. The summary map can also be used to identify the likelihood that each individual observation would benefit a forecast. A flight track may then be modified to optimize use of available observations by moving a few into regions that correspond to higher values of σ^q .

The summary map of Fig. 4a resembles a modulated form of the routine analysis error variance (Fig. 4d) at the targeting time, with its maximum situated along the frontal zone in Fig. 4c. In contrast, Figs. 5a and 5b show an example from NORPEX where the optimal location

for targeting lies in a region where the routine analysis error variance is relatively small. The examples illustrate how the ET KF blends estimates of analysis error variance with information about the growth rate to identify useful observation locations. Optimal ET KF targeting locations often correspond to either (i) regions of very large signal variance at the targeting time, which may not grow as it travels toward the verification region, (ii) regions where the signal variance is initially very small but grows rapidly into the verification region, or (iii) regions of initially high signal variance that grows rapidly into the verification region.

The optimality of targeting locations varies from day to day. The value of adaptive observations in an operational context has been studied by Szunyogh et al. (1999a,b, 2000) and Toth et al. (2000), and summarized in Toth et al. (2001). A quantitative analysis of the ability of ET KF summary maps to identify optimal locations for targeting is still required.

b. Serial targeting

As discussed in Part I, assessing the value of all possible combinations and permutations of several drop-windsonde-equipped aircraft is computationally impractical. A reasonable way to deal with such a situation

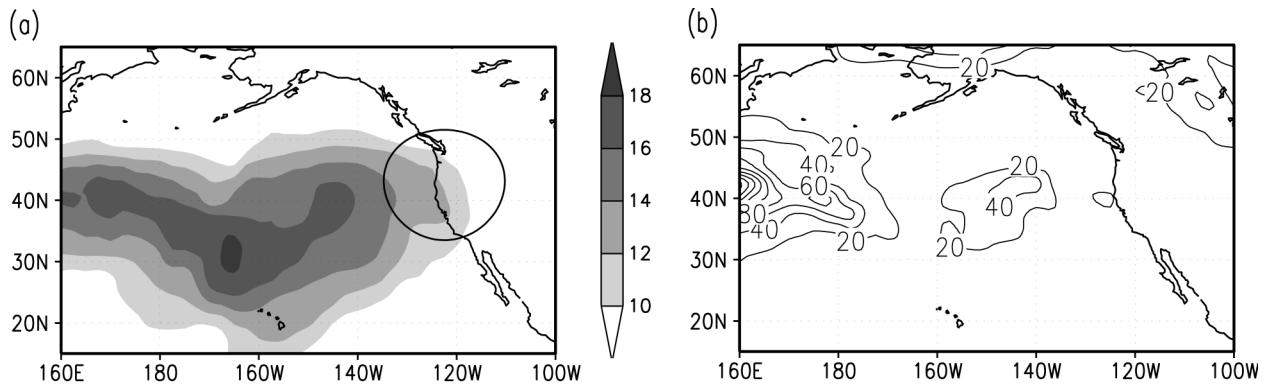


FIG. 5. (a) Summary map of average signal variance σ^q for targeting time 0000 UTC 25 Jan 1998, and verification time 1200 UTC 26 Jan 1998. (b) Routine analysis error variance calculated from transformed 36-h-old ECMWF ensemble perturbations $\mathbf{X}(t_{i+M} | H_i)\mathbf{T}^e$, valid at 0000 UTC 25 Jan 1998.

is to find first the optimal path for one flight and then do likewise for a second flight, *given that observations taken by the first flight were to be assimilated with the ET KF*. During the 2000 WSR program, this technique was employed when more than one aircraft was available for taking observations simultaneously. We demonstrate the use of serial targeting via bar charts of average signal variance σ^q for each possible flight track. In this example, two aircraft were ready for deployment at 0000 UTC 23 January 2000. One forecast situation of concern was a potential storm development in the Gulf of Mexico on 0000 UTC 26 January 2000, based on forecasts issued on 21 January. All available tracks over the northern Pacific (discussed in more detail in Toth et al. 2001) are displayed in Fig. 6a. To identify the first optimal flight, the only background observations assumed are from the routine observational network. Flight track 23 out of Anchorage produces the maximum value of σ^q (Fig. 6b). However, it is not clear from Fig. 6b where a second set of observations ought to be deployed. Some additional observations may turn out to be redundant, given that observations from track 23 are to be assimilated. To identify the second location, we estimate the new background error covariance matrix from (3), using the appropriate form of $\hat{\mathbf{H}}^{23}$ corresponding to track 23. The ET KF can then be used again, assuming this new background error covariance matrix, to identify a new optimal flight path (Fig. 6c). It turns out that track 46 out of Honolulu is now optimal. Although Fig. 6b suggests that tracks such as 1, 8, and 15 would have been reasonable first choices, Fig. 6c indicates that these tracks would not be so effective if track 23 had already been chosen, since some regions that tracks 1, 8, and 15 cover have already been observed by track 23.

If the ET KF or an ensemble Kalman filter were being used to assimilate the data, such a serial targeting strategy would help reduce observational redundancy in the regular network, that is, taking observations that contribute minimally to a signal and its evolution. We do

not recommend that ET KF serial targeting be used to avoid redundant observations when fixed quasi-isotropic first guess error covariances are used in the data assimilation scheme. However, serial targeting may still be of value in testing the ET KF's ability to rank the value of target sites. According to the ET KF, assimilating observations solely from the first flight should consistently produce a larger signal in the forecast aspect of importance than assimilating observations solely from the second flight. One further point worth mentioning is that the signal variance in Fig. 6b seems unusually high compared with that of Fig. 6c. This is another manifestation of the poor quantitative estimation of the routine analysis error covariance matrix. Furthermore, error variance reduction is only calculated within the subspace of ensemble perturbations, and hence errors outside this subspace are ignored. Work is ongoing to quantify the effects of additional individual sondes on signal variance.

It is noteworthy that all of the flights in Fig. 6b produced a significant signal variance, so it appears that no true "null" flight track option with near-zero signal variance existed. Our reasoning for this is as follows. ET KF signals within the verification region at the verification time may be correlated with signals at particular locations at the targeting time. Such correlations may be real or perhaps spurious, due to the limited number of ensemble members used in the ET KF. Furthermore, an ET KF signal that is far from the observation locations at the targeting time may have arisen from spurious correlations, or it may have usefully exploited error covariance information to correct the analysis along an atmospheric structure of low wavenumber. Hence, long-distance correlations may have led to nonzero signal variances within the verification region for all selected flight paths.

The same serial targeting process can also be applied for any number of available flights at different targeting times, by recalculating the background error covariance matrix and signal variance at each iteration to produce

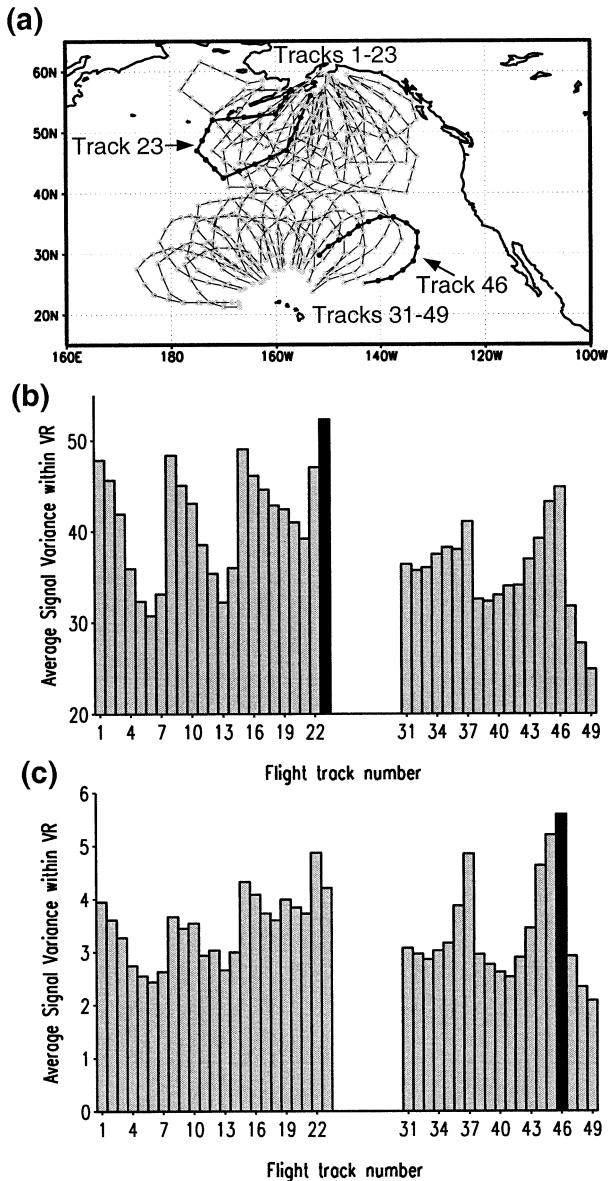


FIG. 6. (a) Map of all predesigned flight paths used during the 2000 WSR program. No flights were officially assigned numbers 24–30. (b) Bar chart of σ^2 for all preselected flight tracks, targeting time 0000 UTC 23 Jan 2000, and verification time 0000 UTC 26 Jan 2000. Verification region of radius 1000 km is centered at 30°N, 90°W. (c) Bar chart of σ^2 for the same set of flight tracks, having already assimilated observations from flight track 23 at the targeting time.

bar charts such as Figs. 6b and 6c. More sophisticated estimates of the analysis error covariance matrix at the targeting times would then be necessary. The theoretical background behind serial assimilation, both in space and in time, is given in section 4 of Part I.

4. ET KF performance during the 2001 WSR program

The concept of signal variance in targeting has been described in the last two sections, with examples se-

lected from recent field programs. In this section, we evaluate the ability of the ET KF to predict (i) the variance of operational signal realizations, and (ii) the effects of targeted observations on reducing forecast error, during the operational 2001 Winter Storm Reconnaissance program, which ran between 23 January and 20 February. The results shown here are produced in a similar manner to Majumdar et al. (2001), who performed the tests for targeted data collected during the 2000 WSR program. They found that a linear, increasing relationship existed between the ET KF and NCEP signal variances, despite major differences between the ET KF and the operational 3DVAR scheme used at NCEP (Parrish and Derber 1992). This relationship held at both the targeting and verification times. Furthermore, a monotonic increasing relationship was found to exist between the variance of operational NCEP signal realizations, and the reduction in NCEP forecast error variance. Hence, Majumdar et al. (2001) concluded that, via a statistical rescaling of the ET KF signal variance, a relationship in principle could be deduced between the ET KF signal variance predictions and the reduction in forecast error variance due to the targeted observations. Since the number of truly independent samples available for testing is small due to the limited number of flights, it is still necessary to test the performance of the ET KF over different periods.

In this section, we summarize the main results for the 2001 WSR program without repeating many details of the statistical tests, which are given in Majumdar et al. (2001). The main difference between our tests and those presented in Majumdar et al. (2001) is that we calculate ET KF signal variance and NCEP signal realizations using the horizontal wind and temperature fields at the 850-, 500-, and 200-hPa levels, whereas Majumdar et al. (2001) only used horizontal wind fields at these levels.

The relationship between the ET KF signal variance and the variance of NCEP signals at the targeting time is displayed in Figs. 7a and 7b. By dividing the data from all 270 observation locations of the 2001 WSR program into five equal bins of 54, in order of increasing ET KF signal variance, sample variances of the NCEP signals at observation sites are calculated in each bin by averaging the squares of the signals (assuming that signal realizations are normally distributed with zero mean). To obtain a statistically significant sample size, all possible data points were used. However, it is open to question whether all realizations are strictly independent of each other, since correlations between signals at two points are related to correlations between the atmospheric states at those points. By plotting the average ET KF signal variance versus the NCEP sample signal variance for each bin, a linear, increasing relationship between ET KF and NCEP signal variances is deduced (Fig. 7b). A rescaling factor of 10 is required at the targeting time; this value is calculated from the slope of the best-fit line and is the factor by which the

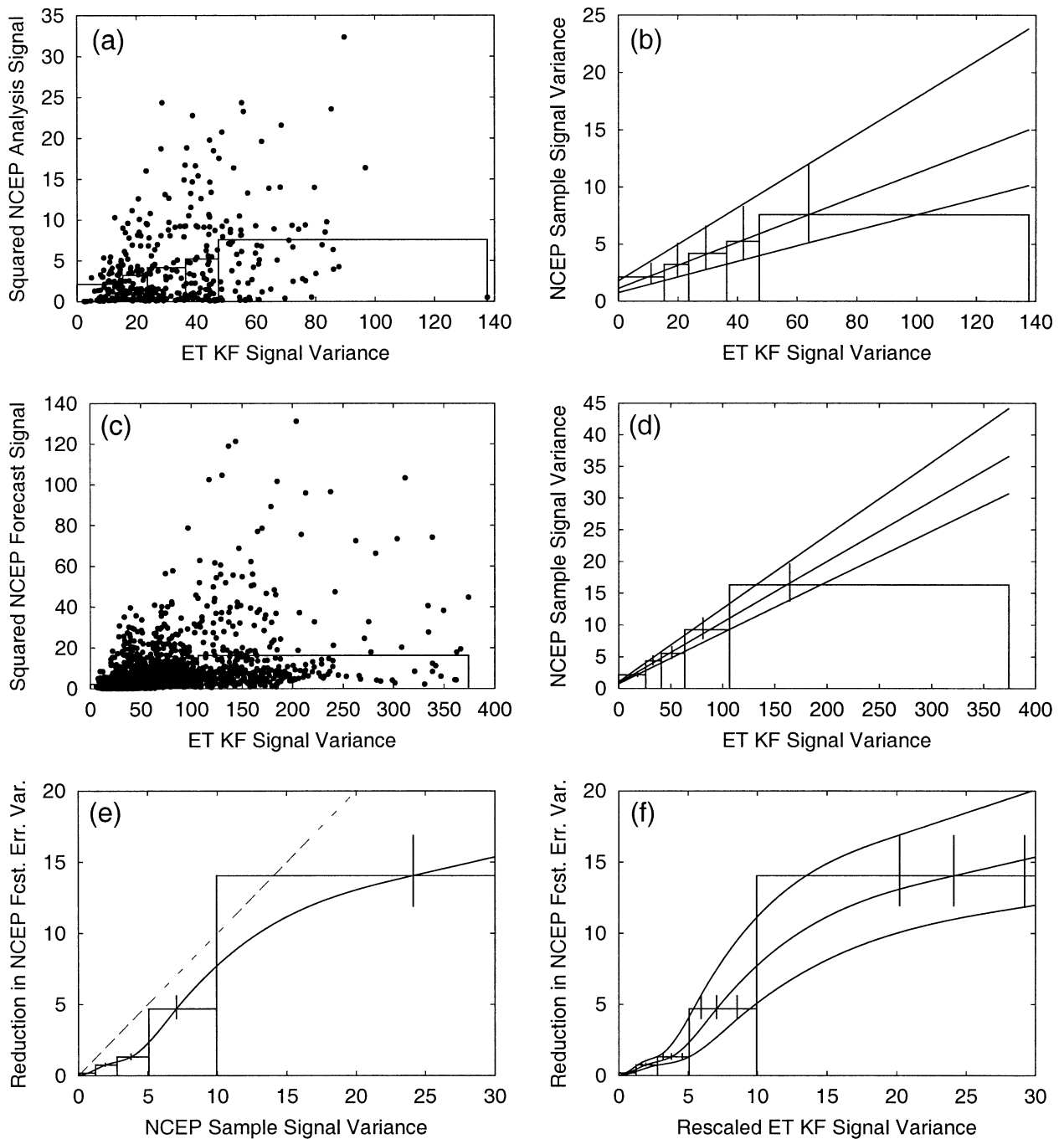


FIG. 7. (a) Scatterplot of squared NCEP signal vs ET KF signal variance for each observation location during the 2001 WSR program, at the targeting time t_{i+M} . The points are divided equally into five bins, arranged in order of increasing ET KF signal variance. The heights of the five bins give the NCEP sample signal variance. (b) Best-fit line and 99% χ^2 confidence intervals for the linear ET KF–NCEP signal variance relationship at the targeting time. (c) As in (a) but for 2015 grid points in all 31 verification regions selected during the 2001 WSR program, at the verification time t_{i+V} . (d) As in (b) but for the verification time. (e) Dashed line, “ideal” relationship between signal variance and reduction in forecast error variance; solid line, actual relationship between NCEP sample signal variance and reduction in NCEP forecast error variance due to the targeted observations, produced in a similar manner to (b) and (d). The 99% χ^2 confidence intervals are shown. (f) Best-fit and confidence intervals for the reduction in NCEP forecast error variance, as a function of rescaled ET KF signal variance. This function is deduced using rescaling factors derived in (d) and the relationship derived in (e).

ET KF signal variance should be reduced. Assuming that the NCEP signal variance in each of the five bins comes from a χ^2 distribution (with 53 degrees of freedom), 99% confidence limits are produced for the NCEP signal variance in each bin as shown in Fig. 7b. By calculating regression lines through the upper limits and the lower limits, the 99% χ^2 interval for the rescaling factor is found to be [6.2, 14.6].

Similarly, a linear, increasing relationship is deduced at the verification time (Figs. 7c,d). The data points correspond to ET KF signal variance and NCEP forecast signal values at all grid points (2.5° resolution) within the 31 verification regions selected during the 2001 WSR program. Again, it is assumed that all signals are independent and normally distributed, with a zero mean. The rescaling factor corresponding to the best-fit line is 10.5, with the 99% χ^2 interval for the rescaling factors ranging between [8.7, 12.5]. These verification cases range from 1-day forecasts on the west coast of the continental United States to 4-day forecasts on the east coast.

The corresponding confidence intervals for the rescaling factor during the 2000 WSR program were [4.1, 11.9] at the targeting time and [11.1, 16.7] at the verification time. The variability of the rescaling factors between the 2000 and 2001 WSR programs is significant, and it is likely due to differences between the selected forecast cases, based upon the dominant flow regimes during each adaptive observing program. For instance, several more forecasts over the eastern United States were targeted during the 2001 WSR program than during the 2000 WSR program. A larger, fully independent, dataset and a more detailed study of forecast cases is required before a rescaling factor can be introduced operationally.

Equation (5e) suggests that the signal variance is equal to the reduction in forecast error variance produced by the targeted observations, provided that errors propagate linearly and error covariances are accurately specified. While this cannot be met in reality, the reduction in NCEP forecast error variance (relative to the NCEP analysis within the verification region) is found to be a monotonic increasing function of NCEP signal variance (Fig. 7e), using the same technique as that described in the previous paragraph for data points within the 31 verification regions. Hence, if the signal variance is large, the chances of a significant reduction in forecast error variance are higher than if the signal variance were small. If the statistical rescaling factors deduced in Fig. 7d are used to rescale the ET KF signal variance, a relationship between the ET KF signal variance predictions and the reduction in NCEP forecast error variance (and the confidence limits) can be deduced as shown in Fig. 7f.

The sensitivity of the above relationships to the removal of subsamples was also tested, using the bootstrapping technique described in Majumdar et al. (2001). In each case, there was usually little variation in the

best-fit line or curve, when samples corresponding to one flight day or one verification region were systematically removed. Hence, the relationships were deemed to be fairly robust. (These results are available from the corresponding author on request.)

The results presented in Fig. 7 demonstrate that, for the second year in a row, the ET KF has shown the ability to predict forecast signal variance, up to a statistical rescaling factor. This ability may be further improved in the near term by introducing a more accurate estimation technique for the routine analysis error covariance matrix than that given in section 2. Potential longer-term implications of the ET KF's ability to predict signal variance and reduction in forecast error variance are discussed in detail in Majumdar et al. (2001). These include (i) discriminating between good and bad days to deploy targeted observations, (ii) warning data quality control schemes not to reject observations if the signal variance is sufficiently large at the targeting time, and (iii) estimating the cost benefit of targeted observations by coupling signal variance predictions with an economic model.

5. Concluding remarks

The ET KF targeting technique superseded the ensemble transform (ET) technique of Bishop and Toth (1999) as the objective strategy used during adaptive observing programs at NCEP. Unlike other current targeting methods, the ET KF estimates the forecast error covariance reducing effect of targeted observations, in advance of the flight preparations.

The current operationally implemented version of the ET KF does not explicitly account for routine observations taken between the ensemble initialization and targeting times. Instead, the ensemble perturbations are transformed at the targeting time so that their magnitudes are consistent with routine analysis error variance estimates, and they are orthogonal with respect to an inverse analysis error variance norm. The analysis error covariance matrix estimated by taking the outer product of these transformed perturbations is then used as the prior or first guess covariance matrix in the prediction of the error reducing effect of additional targeted observations.

By solving the Kalman filter error statistics equations on the ensemble subspace and using serial assimilation theory to break the observational network into routine and targeted observations, the ET KF rapidly estimates the variance of "signals" produced by a future deployment of targeted observations. A signal is defined by the difference between an analysis (forecast) that uses a particular deployment of targeted observations, and an analysis (forecast) that uses no targeted observations. The signal variance is tracked through time, to identify the atmospheric locations in which forecast errors are most likely to be reduced significantly.

We showed how the average signal variance within

a selected verification region could be plotted either as a function of target region location in a summary map, or as a function of prespecified flight tracks in a bar chart. The deployment that maximized this average signal variance was deemed optimal. The bar chart method significantly expedited the flight planning procedure in recent adaptive observing programs. Since the serial assimilation of observations enabled the ET KF targeting results to be produced an order of magnitude faster than the corresponding ET results, several potential forecast situations were assessed before flight instructions were relayed. In the appendix, we demonstrated that the ET KF was able to reproduce ET summary maps if a specific relationship between analysis, background, and forecast error covariances was satisfied.

We also showed how serial assimilation could be used to identify in advance a second optimal deployment of supplementary observations, given that a first deployment had already been issued at that time. Hence, if the error covariances used by the data assimilation scheme were similar to those used by the ET KF, this strategy would allow one to avoid taking redundant observations. However, if the respective error covariances were dissimilar, this approach should be used with caution.

If background and observation error covariances were specified accurately in both the ET KF and the scheme used to assimilate the targeted data, and forecast errors evolved linearly, the signal variance associated with a particular deployment of observations would be equal to the reduction in error variance that would result from taking these observations. However, since forecast errors grow nonlinearly, and error covariances in the operational assimilation scheme and the ET KF are neither similar nor accurately specified, this will not be the case in practice. Despite these limitations, a linear, increasing relationship was found between the ET KF and NCEP signal variances at the targeting and verification times, for the 2001 Winter Storm Reconnaissance program. Additionally, the reduction in NCEP forecast error variance within the verification regions was found to be a monotonic increasing function of the NCEP sample signal variance. Hence, via a statistical rescaling factor, the reduction in forecast error variance could be plotted as a function of the ET KF signal variance. These findings are comparable to similar results produced by Majumdar et al. (2001) for the 2000 WSR program, and provide a benchmark upon which future ET KF-based error covariance estimation techniques must improve. While these results are encouraging, additional research to evaluate the strengths and weaknesses of the ET KF targeting strategy in different flow regimes is necessary.

Further improvements in the ET KF targeting strategy could in principle be achieved by (i) including the observational operator at intervening times between the ensemble initialization and targeting times, (ii) improving routine analysis error covariance estimates, (iii) increasing the number of variables and ensemble members, (iv) making quantitative estimates of signal vari-

ance as a function of the number and spacing of observations, and (v) using a flow-dependent data assimilation scheme in operations that produces error covariances similar to those likely to be produced by an ET KF data assimilation scheme.

Acknowledgments. The authors acknowledge the assistance of Istvan Szunyogh of NCEP in producing the NCEP MRF analysis–forecast cycles, and for his constructive comments. We thank Jonathan Moskaitis of the Pennsylvania State University for handling the data and performing the calculations related to the 2001 Winter Storm Reconnaissance program. We would also like to thank C. Snyder of NCAR and an anonymous referee for their insightful comments and criticisms. S. J. Majumdar, C. H. Bishop, and B. J. Etherton gratefully acknowledge financial support of NSF Grants ATM 96-12502 and ATM 98-14376. S. J. Majumdar is also grateful for the financial support of NOAA Grant NA67RJ0149.

APPENDIX

Conditions under which the ET KF Theory and the ET Formulation of Bishop and Toth (1999) are Equivalent

In the ET KF formulation, two transformations are required to produce the forecast error covariance matrix $\mathbf{P}(t | \mathbf{H}^q)$ at time $t \geq t_{i+M}$ for the q th combined observational network, which comprises the routine network plus the q th deployment of supplementary observations. First the matrix of raw perturbations $\mathbf{X}(t_{i+M} | H_i^r)$ is transformed via (1), assuming a first guess of the inverse analysis error covariance matrix $\mathbf{D}_A^{-1}(\hat{\mathbf{H}}^r)$ of the routine observational network. A second transformation then converts the ensemble perturbations into a form that has assumed the assimilation of the q th set of additional observations. In the ET formulation of Bishop and Toth (1999), a single transformation is performed to map the raw ensemble perturbations to those appropriate for the q th combined observational network. We now prove that this transformation is mathematically equivalent to that of the ET KF, under certain conditions.

The transformation matrices \mathbf{T}^q for the q th combined (routine plus targeted) observational network are defined in Eq. (8) of Bishop and Toth (1999) as solutions to

$$\mathbf{T}^{qT} \mathbf{X}^T(t_{i+M} | H_i^r) \mathbf{D}_A^{-1}(\mathbf{H}^q) \mathbf{X}(t_{i+M} | H_i^r) \mathbf{T}^q = \mathbf{I}. \quad (\text{A1})$$

The \mathbf{C} notation of the transformation matrices in Bishop and Toth is replaced by \mathbf{T}^q for consistency with the formulations in Part I and this paper. The initial guess of the inverse analysis error covariance matrix, based on the combination of routine plus adaptive observations, is given by the $\mathbf{D}_A^{-1}(\mathbf{H}^q)$ term in (A1). Using serial assimilation, we split this matrix into routine and adaptive components to give

$$\mathbf{D}_A^{-1}(\mathbf{H}^q) = \mathbf{D}_A^{-1}(\hat{\mathbf{H}}^r) + \hat{\mathbf{H}}^{qT} \mathbf{R}^{q-1} \hat{\mathbf{H}}^q. \quad (\text{A2})$$

The third term of (A2) explains the error covariances of the q th set of supplementary observations in model space. Furthermore, we require that the transformation matrices \mathbf{T}^q of Bishop and Toth (1999) (and A1) and \mathbf{T}^r in (1) are related by

$$\mathbf{T}^q = \mathbf{T}^r \mathbf{C}^q [\mathbf{\Gamma}^q + \mathbf{I}]^{-1/2}, \quad (\text{A3})$$

where \mathbf{C}^q and $\mathbf{\Gamma}^q$ are as in (4). By substituting (A3) and (A2) into the left-hand side of (A1), the product reduces to the identity matrix, which is the right-hand side of (A1). Hence, the ET KF and ET formulations are equivalent, provided that (A2) and (A3) hold.

REFERENCES

- Baker, N. L., and R. Daley, 2000: Observation and background adjoint sensitivity in the adaptive observation-targeting problem. *Quart. J. Roy. Meteor. Soc.*, **126**, 1431–1454.
- Bergot, T., 1999: Adaptive observations during FASTEX: A systematic survey of upstream flights. *Quart. J. Roy. Meteor. Soc.*, **125**, 3271–3298.
- , G. Hello, A. Joly, and S. Malardel, 1999: Adaptive observations: A feasibility study. *Mon. Wea. Rev.*, **127**, 743–765.
- Bishop, C. H., and Z. Toth, 1999: Ensemble transformation and adaptive observations. *J. Atmos. Sci.*, **56**, 1748–1765.
- , B. J. Etherton, and S. J. Majumdar, 2001: Adaptive sampling with the ensemble transform Kalman filter. Part I: Theoretical aspects. *Mon. Wea. Rev.*, **129**, 420–436.
- Buizza, R., 1995: Optimal perturbation time evolution and sensitivity of ensemble prediction to perturbation amplitude. *Quart. J. Roy. Meteor. Soc.*, **121**, 1705–1738.
- , and A. Montani, 1999: Targeted observations using singular vectors. *J. Atmos. Sci.*, **56**, 2965–2985.
- , T. Petroligis, T. N. Palmer, J. Barkmeijer, M. Hamrud, A. Hollingsworth, A. Simmons, and N. Wedi, 1998: Impact of model resolution and ensemble size on the performance of an ensemble prediction system. *Quart. J. Roy. Meteor. Soc.*, **124**, 1935–1960.
- Evensen, G., 1994: Sequential data assimilation with a non-linear quasi-geostrophic model using Monte Carlo methods to forecast error statistics. *J. Geophys. Res.*, **99** (C5), 10 143–10 162.
- Gelaro, R., R. H. Langland, G. D. Rohaly, and T. E. Rosmond, 1999: An assessment of the singular vector approach to targeted observations using the FASTEX data set. *Quart. J. Roy. Meteor. Soc.*, **125**, 3299–3328.
- , C. A. Reynolds, R. H. Langland, and G. D. Rohaly, 2000: A predictability study using geostationary satellite wind observations during NORPEX. *Mon. Wea. Rev.*, **128**, 3789–3807.
- Gilmour, I., L. A. Smith, and R. Buizza, 2001: Linear regime duration: Is 24 hours a long time in synoptic weather forecasting? *J. Atmos. Sci.*, **58**, 3525–3539.
- Hamill, T. M., and C. Snyder, 2000: A hybrid ensemble Kalman filter–3D variational analysis scheme. *Mon. Wea. Rev.*, **128**, 2905–2919.
- Houtekamer, P. L., and J. Derome, 1994: Prediction experiments with two-member ensembles. *Mon. Wea. Rev.*, **122**, 2179–2191.
- , and H. L. Mitchell, 1998: Data assimilation using an ensemble Kalman filter technique. *Mon. Wea. Rev.*, **126**, 796–811.
- Langland, R. H., and G. D. Rohaly, 1996: Adjoint-based targeting of observations for FASTEX cyclones. *Reprints, Seventh Conf. on Mesoscale Processes*, Reading, United Kingdom, Amer. Meteor. Soc., 369–371.
- , and Coauthors, 1999: The North Pacific Experiment (NORPEX-98): Targeted observations for improved North American weather forecasts. *Bull. Amer. Meteor. Soc.*, **80**, 1363–1384.
- Majumdar, S. J., C. H. Bishop, B. J. Etherton, I. Szunyogh, and Z. Toth, 2001: Can an ensemble transform Kalman filter predict the reduction in forecast-error variance produced by targeted observations? *Quart. J. Roy. Meteor. Soc.*, **127**, 2803–2820.
- Molteni, F., R. Buizza, T. N. Palmer, and T. Petroligis, 1996: The ECMWF ensemble prediction system: Methodology and validation. *Quart. J. Roy. Meteor. Soc.*, **122**, 73–120.
- Palmer, T. N., R. Gelaro, J. Barkmeijer, and R. Buizza, 1998: Singular vectors, metrics, and adaptive observations. *J. Atmos. Sci.*, **55**, 633–653.
- Rabier, F., H. Jarvinen, E. Klinker, J.-F. Mahfouf, and A. Simmons, 2000: The ECMWF operational implementation of four-dimensional variational assimilation I: Experimental results with simplified physics. *Quart. J. Roy. Meteor. Soc.*, **126**, 1143–1170.
- Szunyogh, I., Z. Toth, K. A. Emanuel, C. H. Bishop, C. Snyder, R. E. Mors, J. S. Woolen, and T. P. Marchok, 1999a: Ensemble-based targeting experiments during FASTEX: The effect of dropsonde data from the Lear jet. *Quart. J. Roy. Meteor. Soc.*, **125**, 3189–3217.
- , —, S. J. Majumdar, R. E. Mors, C. H. Bishop, and S. J. Lord, 1999b: Ensemble-based targeted observations during NORPEX. Preprints, *Third Symp. on Integrated Observing Systems*, Dallas, TX, Amer. Meteor. Soc., 74–77.
- , —, R. E. Mors, S. J. Majumdar, B. J. Etherton, and C. H. Bishop, 2000: The effect of targeted dropsonde observations during the 1999 Winter Storm Reconnaissance Program. *Mon. Wea. Rev.*, **128**, 3520–3537.
- Toth, Z., and E. Kalnay, 1997: Ensemble forecasting at NCEP and the breeding method. *Mon. Wea. Rev.*, **125**, 3297–3319.
- , I. Szunyogh, S. J. Majumdar, R. E. Mors, B. J. Etherton, C. H. Bishop, and S. J. Lord, 1999: The 1999 Winter Storm Reconnaissance Program. Preprints, *13th Conf. on Numerical Weather Prediction*, Denver, CO, Amer. Meteor. Soc., 27–32.
- , and Coauthors, 2000: Targeted observations at NCEP: Toward an operational implementation. Preprints, *Fourth Symp. on Integrated Observing Systems*, Long Beach, CA, Amer. Meteor. Soc., 186–193.
- , I. Szunyogh, S. J. Majumdar, C. H. Bishop, and S. J. Lord, 2001: Targeted observations for improving numerical weather forecasts. Preprints, *Fifth Symp. on Integrated Observing Systems*, Albuquerque, NM, Amer. Meteor. Soc., 72–79.
- Wu, W.-S., and S.-W. Joo, 1996: The change of the observational errors in the NCEP SSI analysis. Preprints *11th Conf. on Numerical Weather Prediction*, Norfolk, VA, Amer. Meteor. Soc., 84–85.